Octanuclear Oxothiomolybdate(v) Rings: Structure and Ionic-Conducting Properties

Charlotte du Peloux,[a] Anne Dolbecq,*[a] Philippe Barboux,[b] Guillaume Laurent,[b] Jérôme Marrot,[a] and Francis Sécheresse[a]

Abstract: A family of alkali salts of octanuclear oxothiomolybdate rings has been synthesized by crystallization of the $[Mo_8S_8O_8(OH)_8\{HMO_5(H_2O)\}]^{3-}$ (noted HMo_8M^{3-}; M = Mo, W) and $[Mo_8S_8O_8(OH)_8(C_2O_4)]^{2-}$ (noted Mo_8ox^{2-}) anions in an aqueous solution of ACl (A = Li, Na, K, Rb). Single-crystal X-ray diffraction experiments have been performed showing that the alkali salts exhibit a similar three-dimensional structure. Disordered alkali ions form columns to which the anionic rings are anchored. Ionic-conductivity measurements on pressed pellets have revealed two different behaviors. The lithium salts of HMo_8M^{3-} (M = Mo, W) are moderately good proton conductors at room temperature ($\sigma = 10^{-5}\,S\,cm^{-1}$) and the profile of conductivity as a function of relative humidity shows that the conductivity is due to surface-proton motion (particle-hydrate-type mechanism). On the other hand, the lithium salt of Mo_8ox^{2-} competes with the best crystalline lithium conductors at room temperature ($\sigma = 10^{-3}\,S\,cm^{-1}$), and ^7Li NMR experiments confirm the mobility of the lithium ions along the one-dimensional channels of this material.

Keywords: alkali metals · ionic conductivity · molybdenum · NMR spectroscopy · polyoxometalates

Introduction

Interest in solid, inorganic ionic materials has considerably increased in recent years because of their potential application in various fields, such as hydrogen storage, ion exchange, or catalysis.[1] In particular, lithium-ion conductors attract much attention and a large number of materials have been identified that show sufficiently large conductivities for practical applications in high-energy solid-state batteries.[2] In this respect, novel materials with high conductivities, and explanations of the nature and details of the ionic motion, are required. Finding relationships between the structure and properties of solids can also help in the design of new materials. Our group has recently developed the synthesis of a new family of cyclic oxothiomolybdates, exhibiting various nuclearities and geometries according to the nature of the encapsulated template.[3] These anions crystallize as alkali salts, and the solid-state structures of these salts are sometimes spectacular, from one-dimensional alkali chains[4] to three-dimensional microporous materials.[5] We have recently described the lithium salt of an octanuclear wheel built around a central $W^{VI}O_6$ octahedron.[6] In $Li_3[Mo_8S_8O_8(OH)_8\{HWO_5(H_2O)\}]\cdot 18H_2O$ (noted Li_3HMo_8W), the anions are anchored to lacunary lithium columns. Preliminary ionic-conductivity measurements had shown that this material is a moderately good ionic conductor ($\sigma = 10^{-5}\,S\,cm^{-1}$ at room temperature), and that the main path of conduction involves surface protons rather than lithium ions of the bulk material.[6] The synthetic protocol of $[Mo_8S_8O_8(OH)_8\{HWO_5(H_2O)\}]^{3-}$ has been extended to two other compounds encapsulating a central $Mo^{VI}O_6$ octahedra or an oxalate ($C_2O_4^{2-}$) ligand, and we thus report a complete structural study of the lithium salts of the three anionic wheels and of the different alkali salts of $[Mo_8S_8O_8(OH)_8(C_2O_4)]^{2-}$. The ionic-conduction properties of the whole family and a solid-state ^7Li NMR study of the lithium salts are also presented.

[a] Dr. C. du Peloux, Dr. A. Dolbecq, Dr. J. Marrot, Prof. Dr. F. Sécheresse
Institut Lavoisier, IREM, Université de Versailles Saint-Quentin
45 Avenue des Etats-Unis, UMR 8637
78035 Versailles Cedex (France)
Fax: (+33) 1-39-25-43-81
E-mail: dolbecq@chimie.uvsq.fr

[b] Dr. P. Barboux, G. Laurent
Physique de la Matière Condensée, Ecole Polytechnique
UMR 7643C, 91128 Palaiseau Cedex (France)

Results and Discussion

Structure of the lithium salts of the octanuclear wheels: The HMo_9^{3-} and HMo_8W^{3-} anions have the same overall geometry with C_{4h} symmetry.[6] Four $\{M^V_2S_2O_2\}$ building blocks (M = Mo, W) are connected by hydroxo bridges and encapsulate a central $M^{VI}O_6$ (M = Mo, W) octahedron. The molecular structure of Mo_8ox^{2-} is similar except for a planar oxa-

  DOI: 10.1002/chem.200400068

late ligand that is encapsulated in the octanuclear wheel instead of a MO_6 octahedron.[7] The three lithium salts display a similar three-dimensional structure in which anions and cations are mutually connected and the anionic wheels stack in parallel planes perpendicular to lithium columns (Figure 1). Due to the lower symmetry of the space group

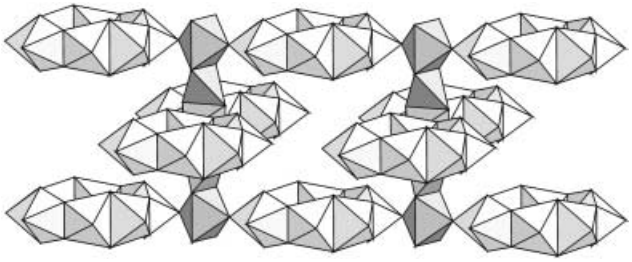

Figure 1. View of the three-dimensional structure of the lithium salts showing the anchoring of the anions to the lithium pillars.

(monoclinic versus quadratic), three crystallographically independent positions for the lithium atoms in the lithium columns were located unambiguously, Li1, Li2A, and Li2B in Li_3HMo_8W,[6] and only two positions, Li1 and Li2, in Li_3HMo_9 and Li_2Mo_8ox. Li1 has a regular tetrahedral coordination while Li2, Li2A, and Li2B are octahedrally coordinated (Table 1). The lithium octahedra and tetrahedra are

Table 1. Selected bond distances [Å].

Lithium salts					
Li_3HMo_8W		Li_3HMo_9		Li_2Mo_8ox	
Li1–O1AW	1.995(12)	Li1–O1W	1.963(1)	Li1–O1W	2.008(3)
Li1–O1BW	1.941(11)				
Li2A–O2A	2.052(5)	Li2–O2	2.075(2)	Li2–O2	2.024(3)
Li2B–O2B	2.134(5)				
Li2A–O1AW	2.175(4)	Li2–O1W	2.185(1)	Li2–O1W	2.281(4)
Li2B–O1BW	2.205(4)				
Li1–Li2A	2.95(2)	Li1–Li2	2.797(1)	Li1–Li2	2.818(1)
Li1–Li2B	2.62(2)				
Alkali salts of Mo_8ox^{2-}					
Na_2Mo_8ox		K_2Mo_8ox		Rb_2Mo_8ox	
Na–O1W	2.271(4)	K–O1W	2.396(4)	Rb1–O2	2.961(9)
Na–O1W	2.797(5)	K–O3	2.890(4)	Rb1–O1W	2.966(16)
Na–O1	3.090(5)	K–O2	3.181(5)	Rb1–O3	3.035(10)
		K–S	3.617(4)	Rb1–O2	3.165(11)
				Rb1–S	3.750(12)
				Rb2–O1W	2.76(3)
				Rb2–O3	2.96(2)
				Rb2–O2	3.03(2)
				Rb2–O3W	3.10(7)
				Rb2–O1	3.29(3)
				Rb2–S	3.83(5)

alternately connected to each other by sharing edges, thus forming a spectacular infinite lithium column (Figure 1) with short Li···Li separations (Table 1). As a full occupancy corresponds to four lithium atoms per anion, the Li columns are only partially occupied. The site-occupancy factors have been determined accurately by using neutron diffraction analyses in Li_3HMo_8W,[6] and with lower accuracy due to lithium being a light element, by using X-ray diffraction analyses for the other two structures (Figure 2). Therefore, in Li_3HMo_8W one half of the octahedral sites are vacant, while in Li_2Mo_8ox all the octahedral sites are vacant, and in Li_3HMo_9 the distribution of the lithium ions in the columns is almost regular.

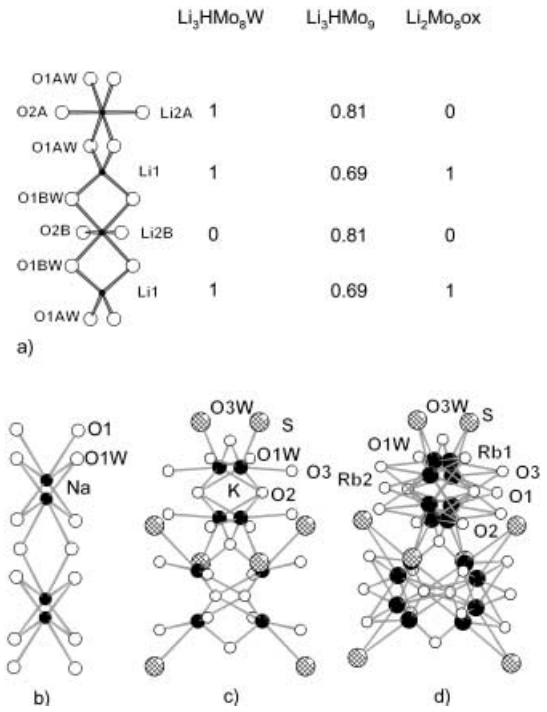

Figure 2. Distribution of the alkali ions: a) lithium ions in the lithium salts with the atom-labeling scheme and the occupancy factors of the lithium ions; in Li_3HMo_8W there are three crystallographically independent lithium sites, Li1, Li2A, and Li2B, while in Li_3HMo_9 and Li_2Mo_8ox A- and B-type sites are equivalent; b) sodium ions in Na_2Mo_8ox; c) potassium ions in K_2Mo_8ox; d) rubidium ions in Rb_2Mo_8ox.

Three-dimensional structure of the sodium, potassium, and rubidium salts of Mo_8ox^{2-}: Surprisingly, the replacement of the lithium cations by alkali cations with a larger ionic radius has little influence on the structure. Indeed, the lithium, sodium, potassium, and rubidium salts are isostructural (Table 2). The anions stack in planes perpendicular to the *c* axis almost identically in each of the four salts (Figure 3), and the cations are connected to the anions and occupy the interstices between the anionic wheels, thus forming infinite chains perpendicular to the molecular plane. The difference lies in the distribution of the alkali cations within the cationic channels. In Li_2Mo_8ox, the lithium cations occupy defined crystallographic sites with octahedral and tetrahedral coordination, the octahedral site being almost empty at room temperature. In Na_2Mo_8ox, the oxo and aquo ligands around the sodium ions define a distorted octahedron, the sodium ion being disordered over two positions on the axis of the column (Figure 2b). In K_2Mo_8ox and Rb_2Mo_8ox, the alkali ions are off-center and delocalized over four and eight positions, respectively, on either side of the axis of the columns

Table 2. X-ray crystallographic data.

	Li_3HMo_9	Li_2Mo_8ox	Na_2Mo_8ox	K_2Mo_8ox	Rb_2Mo_8ox
formula	$H_{49}Li_3Mo_9O_{41}S_8$	$C_2H_{44}Li_2Mo_8O_{38}S_8$	$C_2H_{44}Mo_8Na_2O_{38}S_8$	$C_2H_{34}K_2Mo_8O_{33}S_8$	$C_2H_{34}Mo_8O_{33}Rb_2S_8$
M_r [g]	1846.1	1714.25	1746.35	1688.49	1781.23
crystal system	quadratic	quadratic	quadratic	quadratic	quadratic
space group	*I*4/*m*	*I*4/*m*	*I*4/*m*	*I*4/*m*	*I*4/*m*
Z	2	2	2	2	2
T [K]	296	296	296	296	296
λ [Å]	0.71073	0.71073	0.71073	0.71073	0.71073
a [Å]	14.7749(2)	14.6822(3)	14.7318(5)	14.7257(1)	15.0038(2)
c [Å]	11.1890(2)	11.2735(4)	11.4434(5)	11.4587(1)	11.4927(2)
V [Å^3]	2442.53(6)	2430.19(11)	2483.51(16)	2484.78(3)	2587.17(7)
ρ_{calc} [g cm^{-3}]	2.510	2.343	2.335	2.257	2.287
μ [mm^{-1}]	2.671	2.432	2.398	2.533	4.141
reflections collected	8547	8676	8800	8697	4756
unique reflections (R_{int})	1727 (0.0808)	1738 (0.0378)	1767 (0.0482)	1751 (0.1018)	946 (0.0493)
refined parameters	96	89	92	89	99
$R_1(F_o)$[a]	0.0457	0.0310	0.0433	0.0621	0.0373
$wR_2(F_o^2)$[a]	0.1243	0.0779	0.1215	0.1781	0.1198

[a] $R_1=\frac{\Sigma|F_o|-|F_c|}{\Sigma|F_c|}$; $wR^2=\sqrt{\frac{\Sigma w(F_o^2-F_c^2)^2}{\Sigma w(F_o^2)^2}}$ with $\frac{1}{w}=\sigma^2F_o^2+aP^2+bP$ and $P=\frac{F_o^2+2F_c^2}{3}$; $a=0.0878$, $b=0$ for Li_3HMo_9; $a=0.0435$, $b=2.7241$ for Li_2Mo_8ox; $a=0.0706$, $b=8.7729$ for Na_2Mo_8ox; $a=0.0830$, $b=16.3067$ for K_2Mo_8ox; $a=0.0782$, $b=8.8378$ for Rb_2Mo_8ox.

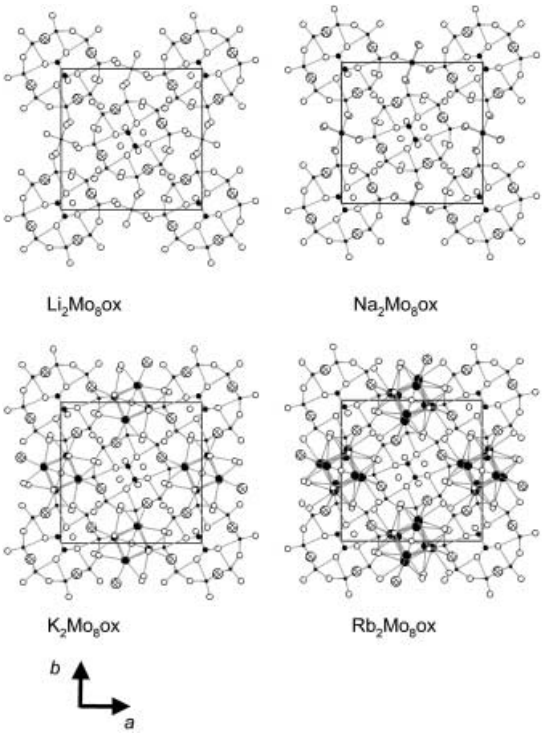

Figure 3. View of the three-dimensional structure of the alkali salts of Mo_8ox^{2-} along the *c* axis, showing the identical disposition of the anionic wheels in the unit cell and the disordered alkali cations in between.

(Figure 2c and 2d). However, the distance between the anionic wheels located in the same plane or in adjacent planes is only slightly modified by the presence of larger cations, as shown by the almost constant values of the *a* and *c* parameters in the series (Table 2).

Clusters of water molecules: In all of the alkali salts, clusters of disordered water molecules are trapped between the holes of the grids. Hydrogen-bonding interactions are found within the cluster of water molecules and between the terminal and bridging oxygen atoms of the polyoxothioanion and adjacent water molecules.[6] In particular, strong O–H···O bonds are present in all the salts between the hydroxo ligands of the anion and water molecules located above and below the molecular plane. This set of hydrogen bonds ensures the cohesion of the inorganic framework and provides a conducting path for proton motion.

Ionic conductivity of the lithium salts: As representative examples, impedance spectra recorded for Li_3HMo_8W are shown in Figure 4 and indicate, from high to low frequency,

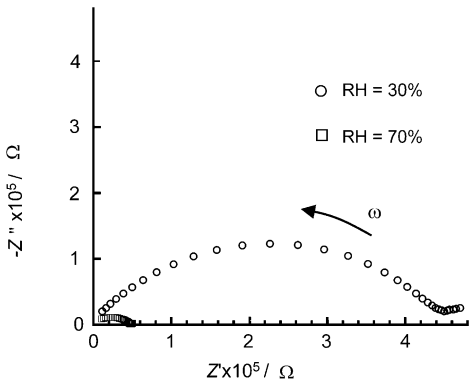

Figure 4. Typical impedance plots obtained at room temperature in two different atmospheres for an Li_3HMo_8W pellet, showing the influence of the relative humidity (RH) on the resistance.

bulk, grain boundary, and electrode-electrolyte effects, the last two being represented here by a single tilted spike. The resistance of the material is determined from the intersection of the first circle with the real Z' axis. We have previously attributed the conductivity to proton rather than lithi-

um motion,[6] the protons coming from the ionization of the oxothioanion or from the dissociation of water molecules, as postulated for alkali salts of $PW_{12}O_{40}^{3-}$ anions.[8] A comparison of the impedance spectra for Li_3HMo_8W recorded under two different atmospheres (Figure 4) shows the importance of the experimental conditions on the values of ionic conductivity and confirms the mechanism of the proton conductivity. The resistance of Li_3HMo_8W is lower, and thus the conductivity higher, when the relative humidity (RH) increases from 30 to 70%, while the weight of the pellet, and thus the number of hydration molecules, remains constant (Figure 5a). A plateau is therefore observed on the

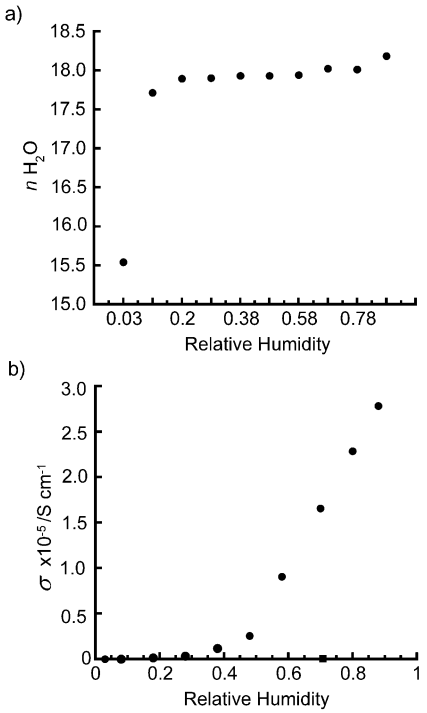

Figure 5. a) Adsorption isotherm of water for Li_3HMo_8W; $n H_2O$ is the number of hydration water molecules. b) Evolution of the conductivity at room temperature versus the relative humidity.

absorption isotherm between 30 and 80% relative humidity (Figure 5a) corresponding to the stoichiometric compound $Li_3[Mo_8S_8O_8(OH)_8\{HWO_5(H_2O)\}]\cdot 18H_2O$. Below that limit there is an abrupt decrease of the amount of water in the compound, and above 80% an additional amount of water is adsorbed. The conductivity is strongly dependent on the partial pressure of water (Figure 5b) and the shape of the curve is typical of a particle-hydrate conductor.[9] These results confirm that the conductivity is mainly due to surface-proton motion.

Impedance measurements have been performed on the other two lithium salts of the family (Figure 6), showing that Li_3HMo_9 and Li_3HMo_8W have similar behavior, while the conductivity of Li_2Mo_8ox at room temperature is higher by two orders of magnitude and is equal to 10^{-3} S cm^{-1}. The conductivity has been studied as a function of temperature in the range −20 to 35 °C. At higher temperatures, a phase transition is observed due to the loss of some hydration water molecules. In this temperature range, the variation of

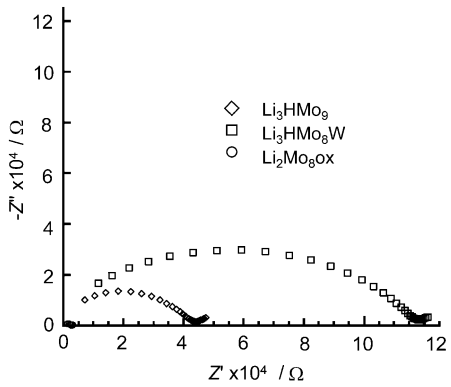

Figure 6. Comparison of impedance plots obtained at room temperature (RH = 70%) for the three lithium salts.

$\log\sigma$ versus $1000/T$ is linear and the conductivity is thermally activated (Figure 7, Table 3), with the exception of Li_2Mo_8ox for which a bend on the curve near $T = -5$ °C is observed. Such a bend corresponds to a jump of activation

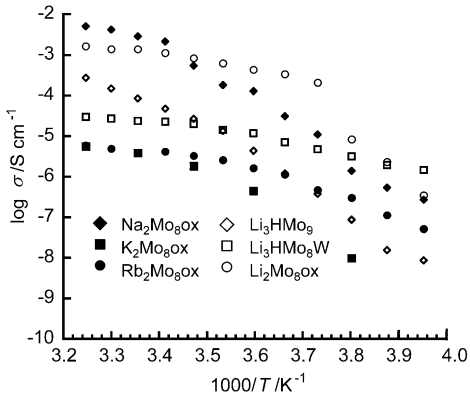

Figure 7. Arrhenius plot of the ionic conductivity between −20 and 35 °C.

Table 3. Conductivities at 20 °C and activation energies measured between −20 and 35 °C for Li_3HMo_8W, Li_3HMo_9, and the alkali salts of Mo_8ox^{2-}, and their comparison with NASICON-type phosphates, LLTO perovskite phases, and heteropoly compounds.

	E_a [eV]	σ [S cm^{-1}]
Li_3HMo_8W	0.47	2.2×10^{-5}
Li_3HMo_9	1.22	4.7×10^{-5}
Li_2Mo_8ox	0.36 ($T=-5$ °C)	1.2×10^{-3}
	1.82 ($T<-5$ °C)	
$Li_2Mo_8ox_{rec}$	0.71	1.4×10^{-5}
Na_2Mo_8ox	1.31	2.1×10^{-3}
K_2Mo_8ox	0.71	4.1×10^{-6}
Rb_2Mo_8ox	1.19	3.7×10^{-6}
$Li_3PW_{12}O_{40}\cdot 13H_2O$[8]	0.45	3.5×10^{-4}
$Li_{1.2}Ti_{1.8}Al_{0.2}(PO_4)_3$ (NASICON)[10]	0.28	5.1×10^{-3}
$(Li_{0.3}La_{0.57}\square_{0.13})TiO_3$ (LLTO)[11]	0.20	1.0×10^{-3}

energy from 0.36 eV at high temperature to 1.82 eV at low temperature and can be connected either with a phase transition or a change in the conduction mechanism.

Li_3HMo_9, with a room temperature conductivity in the order of Li_3HMo_8W and a similar behavior with respect to the relative humidity, is likely a proton conductor, but the

mechanism of ionic conductivity for Li_2Mo_8ox seems different and probably involves the participation of lithium motion. Li_2Mo_8ox has a high ionic conductivity at room temperature and competes with the best-known crystalline lithium-ion-conducting solids (Table 3). Indeed, materials with the NASICON (Na superionic conductor) structure and the formula $[LiM^{IV}_2(PO_4)_3]$ (M = Ge, Ti, Sn, Zr, Hf)[10] or titanium-based perovskite phases $Li_{3x}La_{2/3-x}TiO_3$ (LLTO),[11] have comparable values, both of bulk room temperature conductivities (10^{-3} S cm^{-1}) and activation energies (0.3–0.4 eV).

A striking feature of the lithium salt is that the conductivity of Li_2Mo_8ox is strongly dependent on the experimental conditions. Certainly, the conductivity of a sample which has been recrystallized in 1 M LiCl aqueous solution ($Li_2Mo_8ox_{rec}$) is far lower than that of a nonpurified sample (Table 3). This result is not surprising as it is well known that the conductivity, especially for one-dimensional conductors, is very sensitive to the presence of impurities or structural defects, such as dislocations blocking the channels. In the case of Li_2Mo_8ox, the presence of potassium ions coming from the precursor K_2Mo_8ox has been detected by elemental analysis. We have verified that doping $Li_2Mo_8ox_{rec}$ with a small amount of K_2Mo_8ox improves the conductivity of the sample. A small amount of potassium could lead to a lattice expansion that would favor the lithium motion.

Ionic conductivity of the alkali salts of Mo_8ox^{2-}: The values of conductivity of the A_2Mo_8ox salts are strongly dependent on the nature of the alkaline cation A^+ (Figure 7, Table 3). The salts can be divided into two categories: the good ionic conductors (Li and Na salts) and the poor ionic conductors (K and Rb salts). Na_2Mo_8ox is the best conductor at room temperature, which is not surprising as it is generally known that the small lithium ions are strongly polarizing and thus more strongly solvated and less mobile than the sodium ions. However, the activation energy is surprisingly high for a fast sodium conductor,[12] as activation energies greater than 1 eV are usually encountered with poor ionic conductors.[13] Note also that its conductivity, like Li_2Mo_8ox, depends on the purity of the sample. A pellet of Na_2Mo_8ox recrystallized in a solution of sodium chloride has a lower conductivity by two orders of magnitude than the crude product. Ions with larger ionic radii are probably too large to move in the cationic channels so that K_2Mo_8ox and Rb_2Mo_8ox have low conductivities at room temperature associated with high activation energies.

^{7}Li NMR study: Figure 8 shows the variable-temperature static ^{7}Li NMR spectra ($I = 3/2$) of Li_2Mo_8ox. The spectrum recorded at −50 °C shows the superposition of a broad resonance with a linewidth of approximately 10 kHz and a narrow peak with a linewidth of 500 Hz. As the temperature increases, the broadest peak narrows while the linewidth of the narrowest peak remains unchanged, so that at high temperature the two peaks collapse into a single peak. Concomitantly, the spin-lattice relaxation time (T_1) was measured at different temperatures using a saturation–recovery sequence (Figure 9). There are clearly two different regimes: below −20 °C the T_1 values for the broad and narrow peaks diverge, while at higher temperatures the two resonances have the same spin-lattice relaxation values. This clearly indicates that the broad and narrow peaks originate from two different Li sites and that the peak shape is not due to large quadrupolar interactions. This phenomenon was confirmed by the comparison of the π/2 pulse lengths for Li_2Mo_8ox and a solution of lithium chloride, for which the quadrupolar interactions are weak: both samples have similar π/2 pulse lengths equal to 6.8 and 7 μs, respectively.

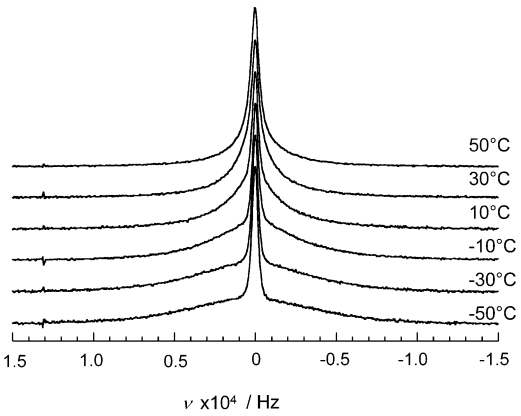

Figure 8. Evolution of ^{7}Li static NMR spectra of Li_2Mo_8ox with temperature.

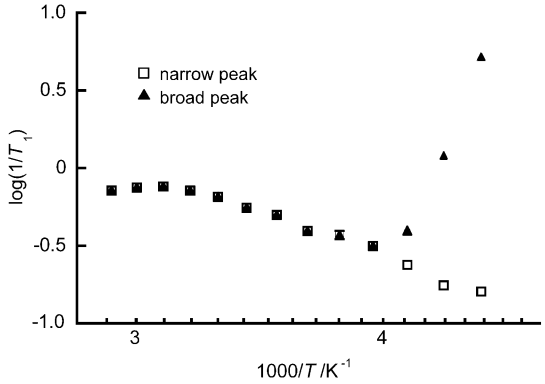

Figure 9. Temperature dependence of the spin-lattice relaxation time $\log(1/T_1)$ for Li_2Mo_8ox.

The most common explanation for the narrowing of a peak upon heating is motional averaging due to an exchange between different lithium sites.[14] The site exchange that causes motional averaging requires the Li^+ ions to hop into a vacant site followed by hopping into a second previously occupied site. Site exchange is thus closely related to ionic conductivity. At room temperature, the ^{7}Li NMR spectra of Li_2Mo_8ox exhibit a single narrow peak, while the spectra of Li_3HMo_8W and Li_3HMo_9 show the superposition of a narrow and a broad peak (Figure 10) correlated to localization of the Li^+ ions. This behavior is consistent with the ionic-conductivity measurements and confirms that the conductivity of Li_2Mo_8ox is mainly due to Li motion, whereas protons are the main mobile ions in the other two lithium salts.

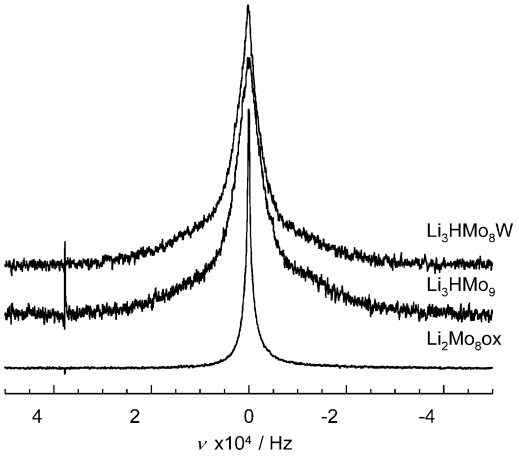

Figure 10. Comparison of the ^{7}Li static NMR spectra recorded at room temperature of Li_3HMo_8W, Li_3HMo_9, and Li_2Mo_8ox.

The attribution of the broad and narrow peaks can be made according to the proposed Li site-occupancy factors (Figure 2). Indeed, in the structure of Li_2Mo_8ox at room temperature the electronic density on the octahedral sites is very weak, which means that the site population is low, or that the lithium ions that occupy this site have large thermal parameters, that is, are mobile.[15] This result is consistent with a high mobility of the lithium ions in octahedral sites, so the broad peak can be attributed to Li ions in octahedral sites, while the narrow peak would be assigned to Li ions in tetrahedral sites. Furthermore, there are three possible mechanisms of line broadening: 1) chemical-shift anisotropy, usually very small for ^{7}Li, 2) quadrupolar interactions, due to the coupling between the nuclear quadrupole moment and fluctuating electric-field gradients created at nuclear sites, and 3) dipolar–dipolar interactions, generated by fluctuating interactions between nuclear magnetic moments of atoms. In the case of dipolar-dominated broadening, the linewidth increases, and the larger the number and the shorter the distance of surrounding Li^+ (homonuclear broadening) and H^+ ions (heteronuclear broadening). It is however, difficult in Li_2Mo_8ox to correlate the linewidth of each site to structural considerations, because there are no clear differences between the octahedral and tetrahedral sites in terms of symmetry (quadrupolar effect) and proximity of Li^+ or H^+ ions (dipolar effect). Note also that, as usually observed, and contrary to what has been described for some zeolites[15,16] or $Li_{2-2x}Mg_{1+x}Cl_4$ spinels,[17] the chemical-shift difference between both sites is negligible, probably because the chemical environments are too close.

^{1}H NMR study: Figure 11 shows the static ^{1}H solid-state NMR spectrum of Li_2Mo_8ox at room temperature. This spectrum shows the superposition of a broad resonance with a linewidth of approximately 20 kHz and a narrow line. The broad peak, which contains the majority of the signal, can be attributed to static protons while the narrow peak, almost negligible, is due to mobile protons. This experiment confirms that in Li_2Mo_8ox only a small portion of the protons are mobile, probably the protons at the surface of the grains and the high-conductivity value is therefore due to one-dimensional lithium motion.

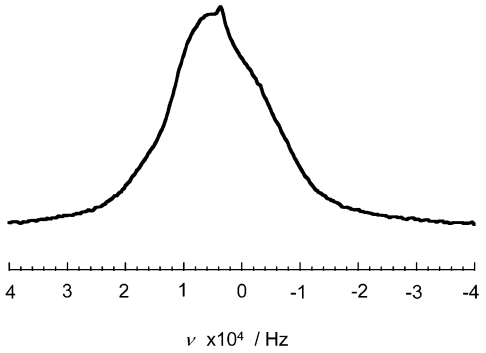

Figure 11. Static ^{1}H solid-state NMR spectrum of Li_2Mo_8ox recorded at room temperature.

Conclusion

In this work we have described a new family of ionic conductors, two of which exhibit fast, one-dimensional ion-conducting properties ($\sigma = 10^{-3}\,S\,cm^{-1}$) at room temperature. Although practical applications are questionable, because of their narrow thermal stability domain and their solubility in most common solvents, these materials are interesting from a fundamental point of view for a study of conduction mechanisms determined by impedance measurements and correlated with ^{7}Li NMR results. Thus, the complementary use of these two techniques has allowed the mechanism for ionic conduction in the three lithium salts to be proposed. In the lithium salt of the oxalate derivative, the main conducting species are the lithium ions, while in the lithium salts of the octanuclear wheels built around a central MO_6 (M = Mo, W) octahedron, the conductivity is dominated by the protons, which move at the surface of the particles. Furthermore, as expected for alkali ionic conductors, ionic conductivity is highest for the sodium salt, which is the best compromise between ionic size and lattice-polarizing character.

Experimental Section

$K_3[Mo_8S_8O_8(OH)_8\{HMoO_5(H_2O)\}]\cdot 15H_2O$ (K_3HMo_9): $Na_2MoO_4\cdot 2H_2O$ (0.78 g, 3.22 mmol) was dissolved in degassed potassium hydroxide (1 M, 60 mL). The crude oxothio precursor $[K_{0.4}(NMe_4)_{0.1}I_{0.5}\{Mo_2S_2O_2(OH)_2\}\cdot 6.3H_2O]_n$ (6 g, 11.2/*n* mmol) was then added. The solution was stirred vigorously until the yellow precursor dissolved to give a dark red solution of $[Mo_2S_2O_2(OH)_4(H_2O)]^{2-}$. The pH was adjusted to 4.5 by dropwise addition of a solution of 4 M HCl. The precipitation of the potassium salt was achieved by cooling the solution in an ice bath. The orange solid was collected by filtration, washed with EtOH, and dried with Et_2O (5.7 g, 93.4% based on Mo). IR (KBr pellets): $\tilde{\nu} = 1060$ (w), 951 (s), 837 (w), 758 (w), 653 (s), 598 (m), 509 (s), 416 (w), 338 cm^{-1} (m); elemental analysis calcd (%) for $H_{41}K_3Mo_9O_{37}S_8$: K 6.27, Mo 46.17, S 13.69; found: K 5.90, Mo 46.23, S 13.36.

$Li_3[Mo_8S_8O_8(OH)_8\{HMoO_5(H_2O)\}]\cdot 25H_2O$ (Li_3HMo_9): K_3HMo_9 (0.5 g, 0.27 mmol) was dissolved in hot water (50 mL, 50 °C). After addition of LiCl (2 g, 4.7×10^{-2} mol), the solution was allowed to stand at room temperature for crystallization. Orange crystals of Li_3HMo_9 suitable for X-ray diffraction studies were collected after several days (0.46 g, 88.2%

based on Mo). IR (KBr pellets): $\tilde{\nu}$ = 1063 (w), 945 (s), 784 (w), 630 (s), 587 (m), 494 (s), 415 (w), 338 cm^{-1} (m); elemental analysis calcd (%) for $H_{61}Li_3Mo_9O_{47}S_8$: Li 1.07, Mo 44.23, S 13.11; found: Li 1.11, Mo 44.16, S 13.10.

$Li_3[Mo_8S_8O_8(OH)_8\{HWO_5(H_2O)\}]\cdot 18H_2O$ (Li_3HMo_8W): The synthesis and characterizations have already been described.[6]

$Li_2[Mo_8S_8O_8(OH)_8(C_2O_4)]\cdot 26H_2O$ (Li_2Mo_8ox): $K_2[Mo_8S_8O_8(OH)_8(C_2O_4)]\cdot 14H_2O$ (0.5 g, 0.29 mmol) was dissolved in hot water (50 mL, 50 °C). LiCl (2 g, 47 mmol) was added and the solution was left for crystallization at room temperature. Orange crystals of Li_2Mo_8ox suitable for X-ray diffraction studies were collected after several days (0.48 g, 89.1 % based on Mo). IR (KBr pellets): $\tilde{\nu}$ = 1099 (w), 958 (s), 789 (m), 623 (w), 517 (s), 417 (w), 340 cm^{-1} (w); elemental analysis calcd (%) for $C_2H_{60}Li_2Mo_8O_{46}S_8$: C 1.29, Li 0.75, Mo 41.33, S 13.78; found: C 1.36, Li 0.74, Mo 40.50, S 14.11.

$Na_2[Mo_8S_8O_8(OH)_8(C_2O_4)]\cdot 26H_2O$ (Na_2Mo_8ox): $K_2[Mo_8S_8O_8(OH)_8(C_2O_4)]\cdot 14H_2O$ (0.5 g, 0.29 mmol) was dissolved in hot water (50 mL, 50 °C). NaCl (2 g, 34.2 mmol) was added and the solution was left for crystallization at room temperature. Orange crystals of Na_2Mo_8ox suitable for X-ray diffraction studies were collected after several days (0.45 g, 82.1 % based on Mo). IR (KBr pellets): $\tilde{\nu}$ = 1101 (w), 958 (s), 790 (m), 666 (w), 519 (s), 418 (w), 342 cm^{-1} (w); elemental analysis calcd (%) for $C_2H_{60}Mo_8Na_2O_{46}S_8$: C 1.27, Mo 40.63, Na 2.43, S 13.55; found: C 1.59, Mo 40.59, Na 2.61, S 14.30.

$K_2[Mo_8S_8O_8(OH)_8(C_2O_4)]\cdot 14H_2O$ (K_2Mo_8ox): The raw powder was synthesized according to previously published procedures.[7a] For growing single crystals, the orange powder (1.5 g) was dissolved in water (200 mL), the solution was heated at 60 °C, and KCl (7.5 g, 0.1 mol) was added. After filtration, the solution was left at room temperature for crystallization. After a week, orange crystals were collected by filtration (1.39 g, 91.4 %). Elemental analysis calcd (%) for $C_2H_{36}Mo_8K_2O_{34}S_8$: C 1.41, Mo 45.22, K 4.59, S 15.08; found: C 1.46, Mo 45.33, K 4.40, S 14.91.

$Rb_2[Mo_8S_8O_8(OH)_8(C_2O_4)]\cdot 14H_2O$ (Rb_2Mo_8ox): $K_2[Mo_8S_8O_8(OH)_8(C_2O_4)]\cdot 14H_2O$ (0.5 g, 0.29 mmol) was dissolved in hot water (50 mL, 50 °C). RbCl (0.15 g, 1.24 mmol) was added and the solution was left for crystallization at room temperature. Orange crystals of Rb_2Mo_8ox suitable for X-ray diffraction studies were collected after several days (0.37 g, 74.4 % based on Mo). IR (KBr pellets): $\tilde{\nu}$ = 1065 (w), 951 (s), 935 (s), 787 (m), 660 (w), 522 (s), 420 (w), 342 cm^{-1} (w); elemental analysis calcd (%) for $C_2H_{36}Mo_8Rb_2O_{34}S_8$: C 1.40, Mo 44.75, Rb 9.98, S 14.93; found: C 1.89, Mo 45.57, Rb 8.98, S 14.54.

Infrared spectra were recorded on an IRFT Magna 550 Nicolet spectrophotometer at 0.5 cm^{-1} resolution by using the technique of pressed KBr pellets.

X-ray crystallography: Intensity data collection was carried out with a Siemens SMART three-circle diffractometer equipped with a CCD detector using $Mo_{K\alpha}$ monochromatized radiation (λ = 0.71073 Å). The absorption correction was based on multiple and symmetry-equivalent reflections in the data set by using the SADABS program[18] based on the method of Blessing.[19] The structure was solved by direct methods and refined by full-matrix least-squares cycles by using the SHELX-TL package.[20] Crystallographic data are given in Table 2. Selected bond distances are listed in Table 1.

Further details on the crystal structure investigations may be obtained from the Fachinformationszentrum Karlsruhe, 76344 Eggenstein-Leopoldshafen, Germany (fax: (+49) 7247-808-666); e-mail: crysdata@fiz-karlsruhe.de) on quoting the depository number CSD-413645 for Li_3HMo_9.

CCDC-229243–229246 contain the supplementary crystallographic data for Li_2Mo_8ox, Na_2Mo_8ox, K_2Mo_8ox, and Rb_2Mo_8ox, respectively. These data can be obtained free of charge via www.ccdc.cam.ac.uk/conts/retrieving.html (or from the Cambridge Crystallographic Data Centre, 12 Union Road, Cambridge, CB2 1EZ, UK; fax: (+44) 1223-336-033; or deposit@ccdc.cam.ac.uk).

Ion-conductivity measurements: Two-probe impedance measurements were carried out by using an HP4192A impedance meter between 10 and 10^7 Hz. Impedance data were collected in the temperature range −20 to 50 °C over cooling and heating cycles. Samples for electrical measurements were prepared as 13 mm diameter pellets of approximately 0.8 mm thickness ($\rho \approx 1.9$ g cm^{-3}). Copper electrodes were applied using Ag conducting paint. The required relative humidity (RH) was obtained by using solutions of sulfuric acid.

^{7}Li NMR experiments: Solid-state NMR analyses were performed on a Bruker MSL 360 spectrometer equipped with a Doty MAS probe operating at Larmor frequencies of 139.96 MHz for ^{7}Li in rotors of 7 mm. The spectra were acquired with delays of 10 s. The relaxation time (T_1) was measured in the temperature range 223–303 K by using both inversion–recovery sequences ($\pi - \tau - \pi/2$) and saturation pulse sequences. The two methods led to the same results.

Acknowledgments

Dr. Dominique Petit (Ecole Polytechnique) is gratefully acknowledged for fruitful discussions on the NMR experiments.

[1] C. N. R. Rao, J. Gopalakrishnan, *New Directions in Solid State Chemistry*, Cambridge, **1997**.
[2] a) A. D. Robertson, A. R. West, A. G. Ritchie, *Solid State Ionics* **1997**, *104*, 1; b) C. A. Vincent, *Solid State Ionics* **2000**, *134*, 159.
[3] E. Cadot, F. Sécheresse, *Chem. Commun.* **2002**, 2189.
[4] E. Cadot, B. Salignac, T. Loiseau, A. Dolbecq, F. Sécheresse, *Chem. Eur. J.* **1999**, *5*, 3390.
[5] E. Cadot, A. Dolbecq, B. Salignac, F. Sécheresse, *J. Phys. Chem. Solids* **2001**, *62*, 1533.
[6] A. Dolbecq, C. du Peloux, A.-L. Auberty, S. A. Mason, P. Barboux, J. Marrot, E. Cadot, F. Sécheresse, *Chem. Eur. J.* **2002**, *8*, 349.
[7] a) A. Dolbecq, B. Salignac, E. Cadot, F. Sécheresse, *Bull. Pol. Acad. Sci. Chem.* **1998**, *46*, 237; b) B. Salignac, S. Riedel, A. Dolbecq, F. Sécheresse, E. Cadot, *J. Am. Chem. Soc.* **2000**, *122*, 10381.
[8] E. A. Ukshe, L. S. Leonova, A. I. Korosteleva, *Solid State Ionics* **1989**, *36*, 219.
[9] P. Barboux, R. Morineau, J. Livage, *Solid State Ionics* **1988**, *27*, 221.
[10] K. Arbi, S. Mandal, J. M. Rojo, J. Sanz, *Chem. Mater.* **2002**, *14*, 1091.
[11] a) Y. Inugama, L. Chen, M. Itoh, T. Nakamura, T. Ushida, H. Ikuta, M. Wakihara, *Solid State Commun.* **1993**, *86*, 689; b) O. Bohnke, J. Emery, J.-L. Fourquet, *Solid State Ionics* **2003**, *158*, 119.
[12] a) F. Brunet, N. Bagdassarov, R. Miletich, *Solid State Ionics* **2003**, *159*, 35; b) D. Mazza, *J. Solid State Chem.* **2001**, *156*, 154; c) O. Bohnke, S. Ronchetti, D. Mazza, *Solid State Ionics* **1999**, *122*, 127.
[13] a) A. Laghzizil, P. Barboux, A. Bouhaouss, *Solid State Ionics* **2000**, *128*, 177; b) A. Daidouh, C. Pico, M. L. Veiga, *Solid State Ionics* **1999**, *124*, 109.
[14] a) J. F. Stebbins, Z. Xu, D. Vollath, *Solid State Ionics* **1995**, *78*, 1; b) C. León, M. L. Lucía, J. Santamaría, M. A. París, J. Sanz, A. Várez, *Phys. Rev. B* **1996**, *54*, 184; c) R. Bertermann, W. Müller-Warmuth, C. Jansen, F. Hiltmann, B. Krebs, *Solid State Ionics* **1999**, *117*, 245.
[15] L. J. Smith, H. Eckert, A. K. Cheetham, *J. Am. Chem. Soc.* **2000**, *122*, 1700.
[16] M. Feuerstein, R. F. Lobo, *Chem. Mater.* **1998**, *10*, 2197.
[17] R. Nagel, C. Wickel, J. Senker, H. D. Lutz, *Solid State Ionics* **2000**, *130*, 169.
[18] G. M. Sheldrick, *SADABS*, *Program for Scaling and Correction of Area-Detector Data*, University of Göttingen, Germany, **1997**.
[19] R. Blessing, *Acta Crystallogr. Sect. A* **1995**, *51*, 33.
[20] a) G. M. Sheldrick, *Acta Crystallogr. Sect. A* **1990**, *46*, 467; G. M. Sheldrick, SHELX-TL version 5.03, Software Package for the Crystal Structure Determination, Siemens Analytical X-ray Instrument Division, Madison, WI, USA, **1994**.

Received: January 20, 2004

Published online: April 29, 2004

